

Feature extraction from light-scatter patterns of *Listeria* colonies for identification and classification

Bulent Bayraktar

Purdue University
Bindley Bioscience Center
Purdue University Cytometry Laboratories
Department of Electrical and Computer Engineering
West Lafayette, Indiana 47907

Padmapriya P. Banada

Purdue University
Molecular Food Microbiology Laboratory
Lafayette, Indiana 47907

E. Daniel Hirleman

Purdue University
School of Mechanical Engineering
Lafayette, Indiana 47907

Arun K. Bhunia

Purdue University
Molecular Food Microbiology Laboratory
Lafayette, Indiana 47907

J. Paul Robinson

Purdue University
Bindley Bioscience Center
Purdue University Cytometry Laboratories
Department of Basic Medical Sciences
School of Veterinary Medicine
and
Weldon School of Biomedical Engineering
West Lafayette, Indiana 47907

Bartek Rajwa

Purdue University
Bindley Bioscience Center
Purdue University Cytometry Laboratories
Department of Basic Medical Sciences
West Lafayette, Indiana 47907

1 Introduction

The identification of bacterial pathogens in a rapid and specific manner is important for applications in biodetection, especially in reducing food-poisoning incidents or counteracting bioterrorism. Conventional identification of bacterial pathogens usually takes 24 to 48 h following the growth of bacteria on an agar plate or in a culture broth, owing to the extent of biochemical or molecular testing required for confirming the identity of the culture. When time and speed are of vital importance, these methods are not sufficient and should be accompanied by rapid prescreening methods, which would pro-

Abstract. Bacterial contamination by *Listeria monocytogenes* not only puts the public at risk, but also is costly for the food-processing industry. Traditional biochemical methods for pathogen identification require complicated sample preparation for reliable results. Optical scattering technology has been used for identification of bacterial cells in suspension, but with only limited success. Therefore, to improve the efficacy of the identification process using our novel imaging approach, we analyze bacterial colonies grown on solid surfaces. The work presented here demonstrates an application of computer-vision and pattern-recognition techniques to classify scatter patterns formed by *Listeria* colonies. Bacterial colonies are analyzed with a laser scatterometer. Features of circular scatter patterns formed by bacterial colonies illuminated by laser light are characterized using Zernike moment invariants. Principal component analysis and hierarchical clustering are performed on the results of feature extraction. Classification using linear discriminant analysis, partial least squares, and neural networks is capable of separating different strains of *Listeria* with a low error rate. The demonstrated system is also able to determine automatically the pathogenicity of bacteria on the basis of colony scatter patterns. We conclude that the obtained results are encouraging, and strongly suggest the feasibility of image-based bio-detection systems. © 2006 Society of Photo-Optical Instrumentation Engineers. [DOI: 10.1117/1.2203987]

Keywords: *Listeria monocytogenes*; pattern recognition; scatterometer; feature extraction.

Paper 05338R received Nov. 10, 2005; revised manuscript received Jan. 12, 2006; accepted for publication Feb. 23, 2006; published online May 19, 2006.

vide preliminary results immediately. Hence, forward light-scattering technology was used in the present research as a novel method for identification of bacterial colonies on agar plates without the need for sample processing or preparation. The colonies analyzed were formed by strains belonging to the genus *Listeria*, a Gram-positive intracellular pathogen. This genus is comprised of six species: *L. monocytogenes*, *L. innocua*, *L. ivanovii*, *L. seeligeri*, *L. welshimeri*, and *L. grayi*. The pathogenic species are *L. monocytogenes* (in humans) and *L. ivanovii* (in animals); all the rest are considered nonpathogenic.¹

The scatter patterns obtained from colonies formed by different species and strains of *Listeria* show noticeable visual differences. In this study, we describe the development and

Address all correspondence to Bartek Rajwa, Purdue University, Bindley Bioscience Center - 1203 W. State Street West Lafayette, IN 47907 United States of America; Tel: (765) 494-0757; Fax: (765) 494-0517; E-mail: brajwa@purdue.edu

demonstration of an efficient feature extraction system, based on orthogonal Zernike moments, which is capable of quantifying the differences in bacterial scatterograms. The use of moments and functions polynomials has previously been associated with pattern recognition,^{2,3} image normalization,⁴ measure of image focus,⁵ and character recognition in computer-vision applications.^{6,7} To the best of our knowledge, the only successful use of these moments for classification of biological images is in the area of location proteomics.⁸⁻¹⁰ The advantages of the quantitative approach in this research are reproducibility, objectivity, robustness, and reliability of measurements and analysis. The identification of bacterial scatterograms was performed via shape analysis implemented using digital image-processing techniques. The process involved three major steps: image preprocessing (mainly image enhancement; e.g., adaptive histogram equalization), feature extraction utilizing Zernike moments (extraction of “best” distinguishable/distinctive properties of the objects/patterns), and discrimination and classification.

2 Methods and Algorithms

2.1 Bacterial Colony Preparation

The bacterial strains used for this study were *L. monocytogenes* ATCC19113, *L. innocua* ATCC33090, *L. ivanovii* ATCC11919, *L. welshimeri* ATCC35897 (obtained from ATCC, Manassas, Virginia), *L. grayi* LM89, *L. grayi* LM37, *L. ivanovii* V12, *L. ivanovii* V199 (obtained from VICAM, Watertown, Massachusetts), *L. monocytogenes* F4393, *L. innocua* F4248 (obtained from USDHHS Centers for Disease Control and Prevention, Atlanta, Georgia), *L. monocytogenes* LCDC81-861, *L. innocua* C3-3(L), *L. ivanovii* LA29, *L. welshimeri* 105(2) to 2(L) (obtained from United States Department of Agriculture (USDA) Agricultural Research Service, Washington, DC), *L. monocytogenes* GG8, *L. seeligeri* LA15, *L. seeligeri* SE31 (obtained from Purdue Department of Food Science culture collection), and *L. innocua* NCTC11288 (obtained from Dr. T. Chakraborty, University of Giessen, Germany). The bacterial cultures were serially diluted in sterile 20-mM phosphate buffered saline (PBS), pH 7.4, so that the dilutions would produce about 30 to 50 colonies per plate. The dilutions were evenly distributed on the surface of brain heart infusion (BHI) agar plates in duplicate and were incubated at 37°C for 18 to 36 h or until the colony reached 1.8 to 2 mm in diameter. The thickness of the colony (along the optical axis) was measured from the surface profile data obtained by a laser triangulation probe (Microtrak II Laser Displacement Sensor System, MTI Instruments Incorporated, Albany, New York), and was typically around 0.3 to 0.4 mm.

2.2 Laser Scatterometer

The scatterometer system was built on an optical breadboard for precise and stable positioning of the optical components. The system included the following major components: a laser diode of 635-nm wavelength (1-mW power); an *x-z* moving stage holding the laser; a Petri-dish holder; a detection screen; and a digital camera (Fig. 1). The laser, the Petri-dish holder, and the detection screen were placed sequentially on the optical path (*y* axis) of the laser beam. The distance from the laser to the Petri-dish holder was 100 mm, and the distance

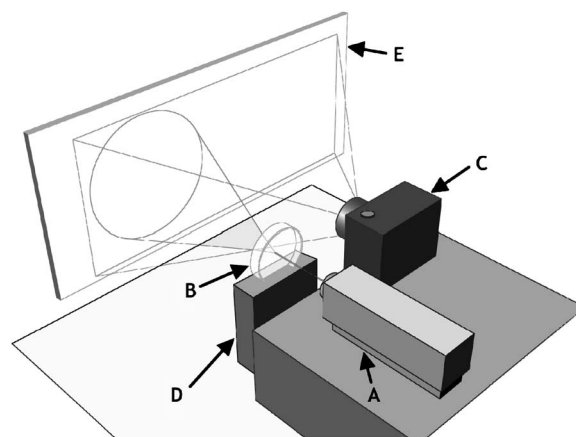


Fig. 1 Schematic representation of the laser scatterometer used to perform analysis of bacterial colonies. (a) 635-nm diode laser, (b) Petri dish containing bacterial colonies, (c) CCD camera, (d) Petri-dish holder, and (e) detection screen.

from the Petri-dish holder to the detecting plane was 280 mm. The laser generated a collimated beam of light on the order of 1 mm in diameter (at the 1/e² irradiance points) that was directed through the center of the bacterial colony, and through the substrate of bacterial agar medium. A portion of the incident light was backscattered from the substrate interfaces and from the bacterial colony, and some was absorbed by the colony. A fraction of the laser beam was also transmitted unscattered through the substrate and through the bacterial colony. Finally, another portion of the incident beam was scattered by the colony in the forward direction (at relatively small angles to the transmitted laser beam). The forward-scattered light and the transmitted light formed the scatter patterns on the detection screen (8×10-in. white board). A digital camera located in the same plane as the Petri-dish holder imaged the scatter patterns.

2.3 Moment Invariants as Features

Features represent scalar properties of imaged objects. In many cases, a small number of features are not sufficient for capturing enough information about an object. Features like area, perimeter, compactness, and Fourier descriptors¹¹ are too simplistic with their limitations (e.g., requirement of clear and closed boundaries), especially for many biological images, and therefore more complex features (e.g., geometric and Zernike moment invariants) found usage ranging from character and face recognition in computer vision to image registration.^{2,7,12-19} In general, moment invariants are tools to quantify the boundary and content characteristics (e.g., shape, pattern) in an image (and hence an object). Desirable properties of moment invariants are orthogonality (orthogonal features will have less redundancy of the image content), low sensitivity to noise (the lower the order of moment, the less sensitive the moment is to noise), low computation complexity (the calculation of features should be efficient enough for real-time applications), good retrieval accuracy (moments can be used to reconstruct the original image), high information content (more information exists about the fine details of an image in higher-order moments), and invariance under photo-

metric (intensity changes) and geometric transformations (e.g., affine transformation, which includes scaling, rotation, translation, etc.).

Appropriate selection of various features to be used for object recognition is one of the key factors in the overall success or failure of the identification and differentiation processes. Selection among features encompasses tradeoffs between their desired properties. For example, a higher order of moment invariant provides more sensitivity but also makes the features more susceptible to noise. Therefore, feature reduction can be performed to select the most distinctive features. Feature reduction can be divided into two categories: feature selection, in which features carrying the most information are picked out through some selection scheme, and feature recombination, in which some features are combined (e.g., with different weights) into a new (independent) feature.

2.4 Zernike Moments and Zernike Moment Invariants

For a 2-D continuous function $f(x,y)$, moments have the general form

$$M_{pq} = \int \int f(x,y)h_{pq}(x,y)dx dy,$$

where $h_{pq}(x,y)$ is a polynomial in x and y with powers p and q , respectively. Zernike moments are represented by a set of complex polynomials, which form a complete orthogonal set over the interior of a circle (i.e., $x^2+y^2=1$): $V_{nm}(x,y) = V_{nm}(r, \theta) = R_{nm}(r)\exp(jm\theta)$, where r is the length of a vector from the origin to an (x,y) pixel, θ is the angle between vector r and the x axis in the counterclockwise direction, n is a non-negative integer, $|m|$ is less than or equal to n subject to the constraint that $n-|m|$ be an even number, and $R_{nm}(r)$ is the radial polynomial:

$$R_{nm}(r) = \sum_{s=0}^{(n-|m|)/2} \frac{(-1)^s(n-s)!}{s! \left[\frac{(n+|m|)}{2} - s \right]! \left[\frac{(n-|m|)}{2} - s \right]!} r^{n-2s}.$$

Note that $R_{n,-m}(r) = R_{n,m}(r)$. These polynomials are orthogonal and satisfy (in 1-D)

$$\int_0^1 R_{nm}(r)R_{n'm}(r)rdr = \frac{1}{2(n+1)} \delta_{nn'}$$

$$\text{with } \delta_{nn'} = \begin{cases} 1 & n = n' \\ 0 & \text{otherwise} \end{cases}.$$

Hence (asterisk * indicates conjugate of a complex number) in 2-D,

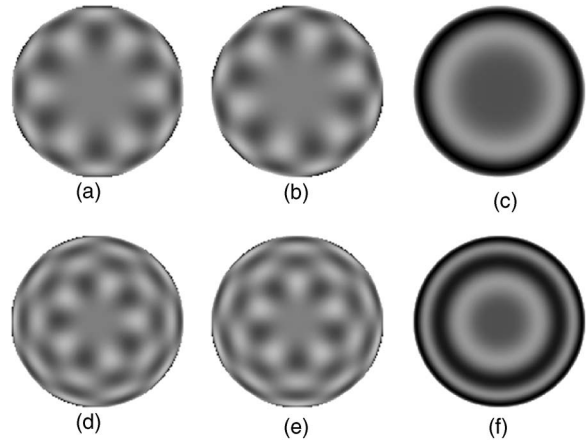


Fig. 2 Graphical representation of radial Zernike polynomials $Z_{n,m}$ in 2-D (image size 128×128 pixels), and their magnitudes: (a) real part $Z_{10,6}$; (b) imaginary part $Z_{10,6}$; (c) magnitude $Z_{10,6}$; (d) real part $Z_{13,5}$; (e) imaginary part $Z_{13,5}$; and (f) magnitude $Z_{13,5}$. The larger the $n-|m|$ difference, the more oscillations are present in the shape. Features used in this study are the magnitudes of Zernike polynomials. One may note that the values of the magnitudes do not change when arbitrary rotations are applied.

$$\int \int_{x^2+y^2 \leq 1} [V_{nm}(x,y)]^* V_{n'm'}(x,y) dx dy = \frac{\pi}{n+1} \delta_{nn'} \delta_{mm'}$$

$$\text{with } \delta_{nn'} = \begin{cases} 1 & n = n' \\ 0 & \text{otherwise} \end{cases}.$$

A Zernike moment^{12-15,19} of order n with repetition m for a continuous image function $f(x,y)$ that vanishes outside the unit circle is defined by

$$Z_{nm} = \frac{n+1}{\pi} \int \int f(x,y) V_{nm}^*(r, \theta) dx dy.$$

For a digital image, the integrals are replaced by summations:

$$Z_{nm} = \frac{n+1}{\pi} \sum_x \sum_y f(x,y) V_{nm}^*(r, \theta), \quad x^2 + y^2 \leq 1.$$

Examples of 2-D Zernike radial polynomials are plotted in Fig. 2. Zernike moments are the projections of the image function onto these orthogonal basis functions. Therefore, if an image has intensity values that are well correlated with the intensity values of one of these polynomials with a specific n and m , the corresponding Zernike moment value is maximized and the distinctive power of this specific Zernike moment invariant reaches its peak.

Application of Zernike moments to the analysis of bacterial scatterograms requires rotational invariance, i.e., their values should not change when arbitrary rotations are applied to the analyzed shapes. Consider a rotation of an image through an angle α . If the rotated image is denoted by f' , the relationship between the original and rotated images in the same polar coordinates is $f'(r, \theta) = f(r, \theta - \alpha)$. The Zernike moment expression can be mapped from the xy plane into polar coordinates by changing the variables in the double integral as¹²

$$\iint \phi(x,y)dx dy = \iint \phi[p(r,\theta),q(r,\theta)] \frac{\partial(x,y)}{\partial(r,\theta)} dr d\theta,$$

where $\partial(x,y)/\partial(r,\theta)$ denotes the Jacobian of the transformation and is the determinant of the matrix.¹²

$$\frac{\partial(x,y)}{\partial(r,\theta)} = \begin{bmatrix} \frac{\partial x}{\partial r} & \frac{\partial x}{\partial \theta} \\ \frac{\partial y}{\partial r} & \frac{\partial y}{\partial \theta} \end{bmatrix}.$$

Here, where $x=r \cos \theta$ and $y=r \sin \theta$, the Jacobian becomes r . Hence,

$$\begin{aligned} Z_{nm} &= \frac{n+1}{\pi} \int_0^{2\pi} \int_0^1 f(r,\theta) V_{nm}^*(r,\theta) r dr d\theta \\ &= \frac{n+1}{\pi} \int_0^{2\pi} \int_0^1 f(r,\theta) R_{nm}(r) \exp(-jm\theta) r dr d\theta. \end{aligned}$$

The Zernike moment of the rotated image in the same coordinates is

$$Z'_{nm} = \frac{n+1}{\pi} \int_0^{2\pi} \int_0^1 f(r,\theta-\alpha) R_{nm}(r) \exp(-jm\theta) r dr d\theta.$$

By a change of variable $\theta_1 = \theta - \alpha$,

$$\begin{aligned} Z'_{nm} &= \frac{n+1}{\pi} \int_0^{2\pi} \int_0^1 f(r,\theta_1) R_{nm}(r) \exp[-jm(\theta_1 + \alpha)] r dr d\theta_1 \\ &= \left[\frac{n+1}{\pi} \int_0^{2\pi} \int_0^1 f(r,\theta_1) R_{nm}(r) \exp(-jm\theta_1) r dr d\theta_1 \right] \\ &\quad \times \exp(-jm\alpha) = Z_{nm} e^{-jm\alpha}. \end{aligned}$$

This analysis shows that under rotation, the argument (orientation angle) of the Zernike moments changes but their magnitude remains unchanged. Therefore, the magnitudes of Zernike moments $|Z_{nm}|$ can be used as invariant features. When n is set to an even number, the total number of Zernike moment invariants (with 0 or positive m) up to n 'th order is $(n^2+4n)/4$. To compute the Zernike moments of a given image, the center of the image is taken as the origin, and pixel coordinates are mapped to the range of the unit circle. Those pixels falling outside the unit circle are not used. An alternative method of calculating Zernike moments is to use a square-to-circular image transformation.¹⁵ Both methods—the unit circle, and the square-to-circular image transformation—were used for Zernike moment calculations presented in this work.

3 Implementation and Results

3.1 Image Collection and Processing

Bacterial colonies with a diameter of approximately 1.8 to 1.9 mm and a thickness of around 0.3 to 0.4 mm (measured along the optical axis) were analyzed using the laser scatterometer. To provide a quantitative and reproducible mathematical description of the patterns, resulting in capability of

discrimination and classification, Zernike moment invariants were used. The circular and mostly symmetric shapes of the observed scatterograms suggested the choice of Zernike moment invariants over other types of moments and their invariants (e.g., Legendre).

Briefly, the original images (640×480 pixels) were cropped to 300×300 pixels by keeping the center of the circularly shaped scatter patterns in the geometric center of the image and selecting a 300×300 rectangle around it. The centering of the patterns was necessary, since Zernike moments in the form utilized for the purpose of this project were not translation invariant. The automated centering process used zero- and first-order geometric moments for finding the centroid of the pattern. After adaptive histogram equalization (*adaphstetq* function in Matlab) was performed on the cropped grayscale images of the scatter patterns, Zernike moment invariants of up to 20th order were calculated. The resultant 120 features describing each image were used as inputs for the analysis procedure. The order of Zernike moment-based features was high enough to include not only low-frequency shape information, but also high-frequency features (details) of the light-scatter patterns. Feature reduction via linear discriminant analysis (LDA) and principal component analysis (PCA) was performed to plot the data in 2-D and visualize clusters, representing different bacterial colonies. After the calculation of principal components, hierarchical clustering was performed to verify the feasibility of automated discrimination of bacterial species and strains. Simple classification was performed using linear discriminant analysis (LDA), partial least squares (PLS), and neural networks (NNs).²⁰ Feature reduction, clustering, classification, and plotting were executed using JMP Statistical Discovery software (SAS Institute Incorporated, Cary, North Carolina).

3.2 Results

Approximately 2000 scatter patterns were collected for the present study. In general, scatter patterns of bacterial colonies were point symmetric and composed of a number of diffraction rings. The point-symmetric characteristic was expected, since the bacterial colonies analyzed were symmetric (dome shaped) and the incident laser beam was pointed at the centers of the colonies. In the majority of scatterograms, a spot at the center of the pattern was observed. However, this spot was absent in some strains, or appeared diffuse in some others. The size and sharpness of the central spot varied in scatterograms obtained from different strains. Typically, at least one ring surrounding the central spot was observed; for some strains there were two, three, or more rings. The size, thickness, sharpness, and intensity of the ring(s) varied. A diffuse pattern around the innermost ring was observed in some scatterograms. In some other images, radial spokes were present outside the innermost ring. The intensity of the whole scatter pattern also varied from strain to strain. Representative images of some analyzed strains are shown in Fig. 3.

For the purpose of this work, three sets of Zernike moment-based features extracted from the bacterial scatterograms were analyzed. In the initial analysis, a single strain of bacteria was chosen to represent the species. From the available images of that strain, 9 to 20 measurements were selected at random. 120 feature vectors were extracted from each of

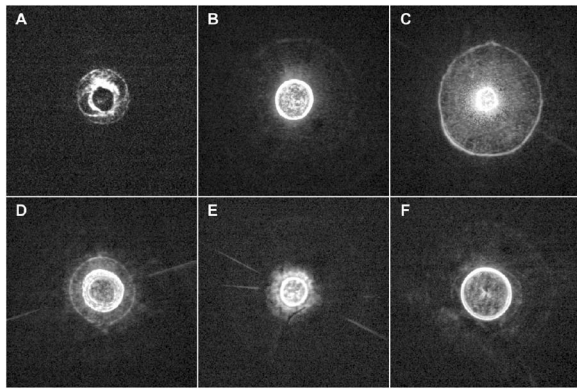


Fig. 3 Representative images of scattergrams produced by six different *Listeria* strains from six species [(a) *L. grayi* LM37, (b) *L. innocua* C3-3(L), (c) *L. ivanovii* V12, (d) *L. monocytogenes* GG8, (e) *L. seeligeri* SE21, and (f) *L. welshimeri* 105(2)-2L]. The pathogenic species are *L. monocytogenes* (in humans) and *L. ivanovii* (in animals); all the rest are considered nonpathogenic. *L. monocytogenes* and *L. innocua* are known to be closely related phylogenetically, and the scattergrams produced by these two bacterial species are indeed the most similar visually.

these images. Using the first five principal components of the feature vectors, we were able to separate each of the species (*L. monocytogenes*, *L. innocua*, *L. ivanovii*, *L. grayi*, *L. seeligeri*, and *L. welshimeri*) by performing hierarchical clustering using Ward's distance (Fig. 4). One may note that although *L. monocytogenes* and *L. innocua* are known to be phylogenetically related,²¹ the scattergrams produced by colonies of the two strains of *L. monocytogenes* and *L. innocua* used in this experiment were clearly distinguishable on the PCA plot (Fig. 5).

To explore further the possibility of discriminating among closely related species, we analyzed a more complex set of data (68 observations) containing three different strains of *L. monocytogenes* and three different strains of *L. innocua*. The hierarchical clustering separated the analyzed strains modestly well, although some errors were noted (Figs. 6 and 7). Observations of *L. innocua* ATCC33090 and *L. innocua* C3-3(L) were assigned to the same cluster. Most importantly, some scattergrams of *L. innocua* C3-3(L) (a nonpathogenic strain of *Listeria*) were assigned to the cluster containing *L. monocytogenes* GG8 (a pathogenic strain). In the next and last step, a simple classification task was attempted. 12 batches of samples for each of 15 different strains [*L. monocytogenes* ATCC19113, *L. monocytogenes* F4393, *L. monocytogenes* LCDC81-861, *L. grayi* LM37, *L. grayi* LM89, *L. seeligeri* LA15, *L. seeligeri* SE31, *L. innocua* NCTC 11288, *L. innocua* C3-3(L), *L. innocua* F4248, *L. ivanovii* ATCC11919, *L. ivanovii* LA29, *L. ivanovii* V12, *L. welshimeri* 105(2)-2(L), and *L. welshimeri* ATCC35897] were randomly chosen, forming a 180-observation set. Our training/testing method involved using 165 observations as a training set and the remaining 15 observations as a test set. 12 different combinations of the training set and test set were utilized. The dataset was divided into three categories representing non-pathogenic *Listeria*, bacteria potentially pathogenic to humans (three strains of *L. monocytogenes*), and bacteria potentially pathogenic to animals (three strains of *L. ivanovii*). Classifi-

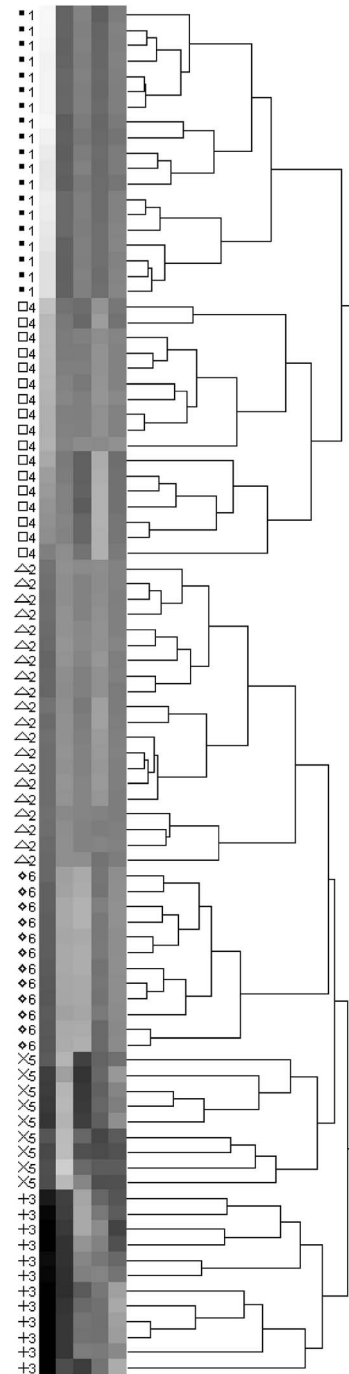


Fig. 4 Hierarchical clustering of bacterial scatter patterns represented on a dendrogram. The vertical axis is made up of the first five principal components describing bacterial scattergrams, and the horizontal axis represents the clusters formed at each step of the clustering procedure. Links (similarities) between objects are shown as U-shaped lines, where the length of the U arms corresponds to the distance. The clustering was performed using Ward's method, where objects and clusters are merged when the increase in within-group variance was less than it would have been if any of the two linked clusters were joined with other existing clusters. Symbols represent six different strains of *Listeria* belonging to six species: ■ *L. grayi* LM37, □ *L. seeligeri* LA15, △ *L. welshimeri* ATCC35897, ◇ *L. monocytogenes* ATCC19113, + *L. innocua* F4248, × *L. ivanovii* V199. Numbers represent identified clusters of patterns. Note that identified clusters coincide with the groups of colonies from different strains.

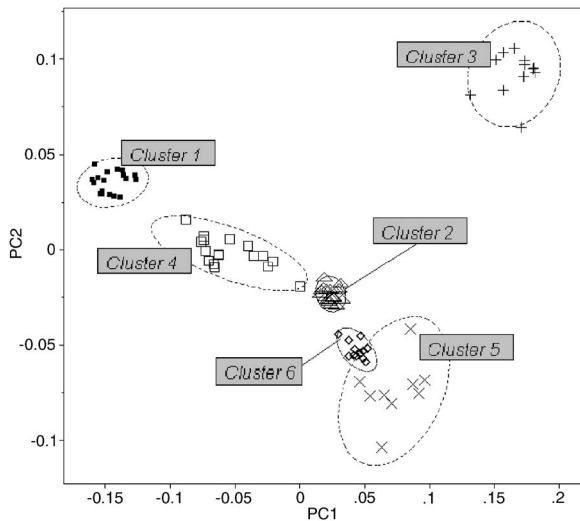


Fig. 5 Scatter pattern of six strains of *Listeria* visualized in principal components plot. Symbols represent the same six strains of *Listeria* as in Fig. 4. Cluster numbers represent sets of patterns identified using the hierarchical clustering method.

cations based on LDA, PLS, and standard (not backpropagated) NNs with three hidden nodes were performed in the environment of the JMP 5.1 package.

For the purpose of classifying observations by PLS and NNs, a dummy matrix in which each element is either zero or one, depending on the pathogenicity of the sample, encoded the information about the bacteria. The dummy matrix can be interpreted as a pseudo-probability matrix representing the probability that a scatterogram identifies a colony that belongs to a particular class. Regression vectors generated from training spectra were used to predict the pseudo-probabilities associated with a given test sample. As with a real probability, the sum of the pseudo-probability scores for all of the possible classes is equal to one. However, unlike true probabilities, individual pseudo-probability scores may be either larger than one or smaller than zero.²² The results of the classification are summarized in Table 1.

The example presented in Fig. 8 shows 30 scatter patterns classified using the NNs system via the procedure described before. The classified patterns are shown as crosses, while the patterns belonging to the training set are shown as filled squares. 84% of patterns are correctly classified in the example presented. Misclassified patterns are shown as filled circles.

4 Discussion and Future Work

The Zernike moment-based feature extraction tool provided up to 120 features for every scatterogram collected. Use of these features either directly or after dimensionality reduction via PCA allowed discrimination and classification of bacterial colonies forming the scatter patterns. Patterns produced by strains belonging to different species of *Listeria* were easily distinguished by a hierarchical clustering method, as demonstrated in Fig. 4. Discrimination of patterns in a mixture of observations belonging to *L. innocua* and *L. monocytogenes* posed a much more difficult problem, as indicated by only a modest discrimination success achieved by hierarchical clus-

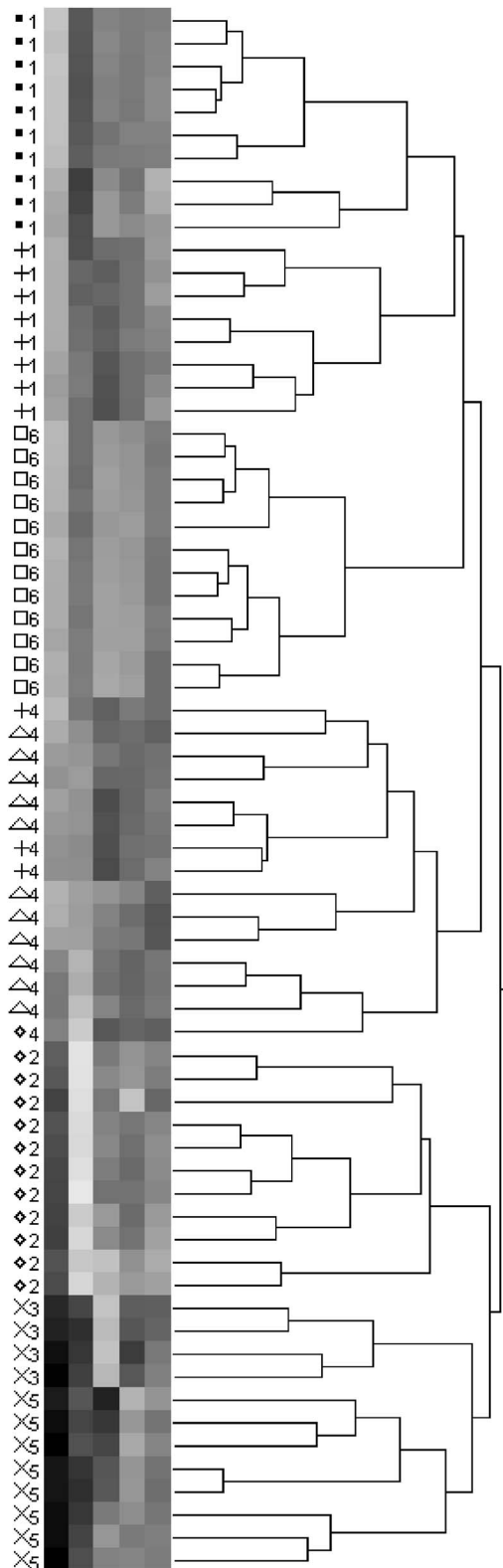


Fig. 6 Hierarchical clustering of scatter patterns produced by bacteria belonging to *L. innocua* and *L. monocytogenes* species. Symbols represent six different strains of *Listeria*: ■ *L. innocua* ATCC33090, □ *L. monocytogenes* ATCC19113, △ *L. monocytogenes* GG8, ◇ *L. monocytogenes* F4393, + *L. innocua* C3-3(L), × *L. innocua* F4248. Numbers represent identified clusters of patterns. Note that some patterns belonging to different strains were assigned to the same cluster.

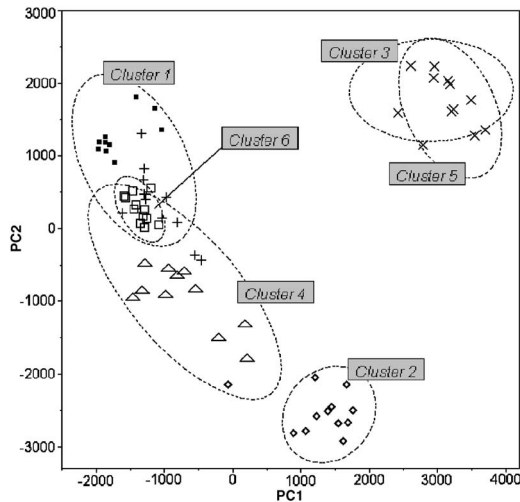


Fig. 7 Principal components plot illustrating hierarchical clustering of scatter patterns produced by colonies of the same six strains of *Listeria* as in Fig. 6.

tering (Fig. 6). This is not surprising, since phylogenetic studies have shown that *L. monocytogenes* and *L. innocua* are closely related.²³ To confirm whether features extracted from scatterograms could be employed for more complex purposes, such as automated pattern recognition, a simple classification procedure using three classes (nonpathogen, human pathogen, and animal pathogen) was performed. Classification success

Table 1 Classification rates for human-pathogenic, animal-pathogenic, and nonpathogenic *Listeria* strains. Classification results of different methods using 180 images from 15 different *Listeria* strains.

Imaged scatterogram	Classified as		
	Human pathogen	Animal pathogen	Nonpathogenic
<i>Classified by PLS</i>			
Human pathogen	66.67%	2.78%	30.56%
Animal pathogen	0.00%	94.44%	5.56%
Nonpathogenic	0.93%	0.93%	98.15%
<i>Classified by NNs</i>			
Human pathogen	75.00%	5.56%	19.44%
Animal pathogen	8.33%	88.89%	2.78%
Nonpathogenic	9.26%	3.70%	87.04%
<i>Classified by LDA</i>			
Human pathogen	66.67%	8.33%	25.00%
Animal pathogen	11.11%	77.78%	11.11%
Nonpathogenic	15.74%	5.56%	78.70%

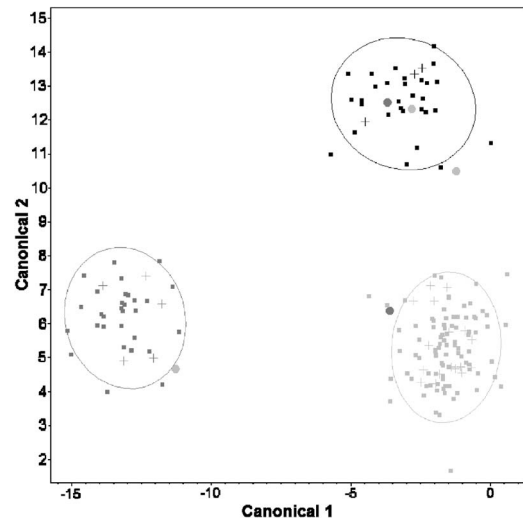


Fig. 8 An example of bacterial pattern classification using a neural networks approach. 30 scatter patterns belonging to 15 different strains representing three groups of bacteria (pathogenic for humans (black, top-right corner of the plot), for animals (dark gray, left side of the plot), and nonpathogenic (light gray, bottom-right corner of the plot)) were classified. The data points are visualized in a canonical plot. The classified patterns are shown as crosses, while the patterns belonging to the training set are shown as filled squares. 84% of patterns are classified correctly in the example presented. Misclassified patterns are shown as filled circles.

varied greatly and depended on the method used. Although 98% of nonpathogenic species were correctly classified with the PLS-based approach, as many as one third (33%) of pathogenic colonies were misclassified. NNs-based classification gave better results, correctly classifying 75% of human pathogens and 88% of animal pathogens. It is important to note that the classification tools used were relatively simple (LDA, PLS, not-backpropagated NNs), and there was no additional penalty for false negatives (i.e., classifying pathogenic strain as a nonpathogenic).

On the basis of the performed clustering and classification, Zernike moment-based features extraction applied to the problem of bacterial scatterograms represents a promising approach to identification of colony-forming bacterial pathogens. The most important problem faced during the analysis was the “curse of dimensionality” resulting from the large number of features and low number of observations (scatterograms) per strain. This is the reason that for the purposes of classification, bacterial scatterograms were divided into just three categories, and prediction of actual strain on the basis of an observed scatterogram was not attempted at this point. The limited success of classification might have arisen from two fundamental limitations in the design of orthogonal Zernike moments: 1. the discrete approximation of the continuous integrals (i.e., scatterograms are discrete images and therefore the analyses must be done using discretized orthogonal moments^{18,19}), and 2. the transformation of the Cartesian scatterogram coordinate system into the domain of the radial polynomials.^{16,19,24} The discrete approximation of integrals affected the analytical properties that the moment functions were intended to satisfy, such as invariance and orthogonality. The coordinate-space normalization increased the computa-

tional complexity. Discrete orthogonal moments (formed from discrete orthogonal polynomials as basis functions) may eliminate the need for numerical approximations and will exactly satisfy the orthogonality property in the image coordinate space. In contrast to Zernike moments, inherently orthogonal and discrete radial Chebyshev moments,²⁴ based on discrete radial Chebyshev polynomials, eliminate the discretization errors. Radial Chebyshev moments are also rotation invariant and can be viewed as discrete counterparts of Zernike moments. Therefore, the application of Chebyshev moments may improve the overall performance of analysis. The authors are currently designing a new pattern classification system utilizing the capabilities of radial Chebyshev moment invariants. Improvement in feature extraction may result in a method capable of fast quantitative characterization of bacterial colonies not only for purposes of biodetection, but also to provide information about changes in bacterial colonies over time or as the result of exposure to various environmental factors. We are currently modifying the new setup and developing an improved version of the pattern recognition system to eliminate some of the shortcomings and problems encountered in this research.

5 Conclusions

This study explores analysis of scatter patterns produced by colonies of different *Listeria* species and strains when irradiated with red laser light. The interaction between the laser beam and the bacterial colony occurs at multiple length scales. At the microscopic end there is scattering by individual bacteria, and at the larger end there is a macroscale lens-like refraction of the beam by the curved free surface of the colony. The nominal 1-mm beam diameter of the diode laser happens to be convenient, since no focusing optics is required and the topography illuminated by the beam allows substantial discrimination among the bacteria we studied. While we have not yet carefully explored the lower limit of beam size, we are convinced that smaller beam sizes could provide similar sensitivity and should be explored. Smaller beam sizes imply that smaller regions of the colonies are required, which in turn means that shorter incubation times would be possible.

The presented method offers a novel, unique approach to the problem of differentiating bacterial colonies by using moment invariants to describe the scatter patterns. Although the complexity of calculating moment invariants for large images is high, given the speed of current computers it is not prohibitive. Moment invariants are robust, and their use has been successfully demonstrated in a number of computer-vision applications. Taking into consideration the fact that providing precise taxonomy of bacterial patterns would not be required during rapid prescreening, we can conclude that the results obtained for automated determination of pathogenicity are encouraging and strongly suggest the feasibility of image-based biodetection systems.

Acknowledgments

We thank Purdue University Cytometry Laboratories staff for their fruitful discussions. In particular, we thank Valery Patsekina for discussions on multivariate analysis. We also acknowledge Songling Guo for his contributions to the initial

setup and data collection. Arun Bhunia would like to acknowledge support through a cooperative agreement with the Agricultural Research Service of the United States Department of Agriculture project number 1935-42000-035 and the Center for Food Safety and Engineering at Purdue University.

References

1. A. J. Roberts and M. Wiedmann, "Pathogen, host and environmental factors contributing to the pathogenesis of listeriosis," *Cell. Mol. Life Sci.* **60**, 904–918 (2003).
2. M. Hu, "Visual-pattern recognition by moment invariants," *IRE Trans. Inf. Theory* **8**, 179–187 (1962).
3. M. R. Teague, "Image-analysis via the general-theory of moments," *J. Opt. Soc. Am.* **70**, 920–930 (1980).
4. Y. S. Abumostafa and D. Psaltis, "Image normalization by complex moments," *IEEE Trans. Pattern Anal. Mach. Intell.* **7**, 46–55 (1985).
5. P. T. Yap and P. Raveendran, "Image focus measure based on Chebyshev moments," *IEE Proc. Vision Image Signal Process.* **151**, 128–136 (2004).
6. L. C. Glenn and H. Mehdi, "Optical character recognition by the method of moments," *Comput. Vis. Graph. Image Process.* **39**, 291–310 (1987).
7. J. Flusser and T. Suk, "Affine moment invariants—a new tool for character-recognition," *Pattern Recogn. Lett.* **15**, 433–436 (1994).
8. M. V. Boland and R. F. Murphy, "A neural network classifier capable of recognizing the patterns of all major subcellular structures in fluorescence microscope images of HeLa cells," *Bioinformatics* **17**, 1213–1223 (2001).
9. R. F. Murphy, "Cytomics and location proteomics: Automated interpretation of subcellular patterns in fluorescence microscope images," *Cytometry* **67A**, 1–3 (2005).
10. R. F. Murphy, "Location proteomics: a systems approach to subcellular location," *Biochem. Soc. Trans.* **33**, 535–538 (2005).
11. R. C. Gonzalez, R. E. Woods, and S. L. Eddins, *Digital Image Processing Using MATLAB*, Pearson Prentice Hall, Upper Saddle River, NJ (2004).
12. A. Khotanzad and Y. H. Hong, "Invariant image recognition by Zernike moments," *IEEE Trans. Pattern Anal. Mach. Intell.* **12**, 489–497 (1990).
13. S. X. Liao and M. Pawlak, "On the accuracy of Zernike moments for image analysis," *IEEE Trans. Pattern Anal. Mach. Intell.* **20**, 1358–1364 (1998).
14. R. Mukundan and K. R. Ramakrishnan, "Fast computation of Legendre and Zernike moments," *Pattern Recogn.* **28**, 1433–1442 (1995).
15. R. Mukundan and K. R. Ramakrishnan, *Moment Functions in Image Analysis—Theory and Applications*, World Scientific, Singapore (1998).
16. R. Mukundan, S. H. Ong, and P. A. Lee, "Image analysis by Tchebichef moments," *IEEE Trans. Image Process.* **10**, 1357–1364 (2001).
17. R. Mukundan, "Some computational aspects of discrete orthonormal moments," *IEEE Trans. Image Process.* **13**, 1055–1059 (2004).
18. C. H. Teh and R. T. Chin, "On digital approximation of moment invariants," *Comput. Vis. Graph. Image Process.* **33**, 318–326 (1986).
19. C. H. Teh and R. T. Chin, "On image-analysis by the methods of moments," *IEEE Trans. Pattern Anal. Mach. Intell.* **10**, 496–513 (1988).
20. R. O. Duda, P. E. Hart, and D. G. Stork, *Pattern Classification*, Wiley, New York (2001).
21. B. Sallen, A. Rajoharison, S. Desvarenne, F. Quinn, and C. Mabilat, "Comparative analysis of 16S and 23S rRNA sequences of *Listeria* species," *Int. J. Syst. Bacteriol.* **46**, 669–674 (1996).
22. C. Ortiz, D. M. Zhang, Y. Xie, V. J. Davissou, and D. Ben Amotz, "Identification of insulin variants using Raman spectroscopy," *Anal. Biochem.* **332**, 245–252 (2004).
23. S. Cai and M. Wiedmann, "Characterization of the prfA virulence gene cluster insertion site in non-hemolytic *Listeria* spp.: Probing the evolution of the *Listeria* virulence gene island," *Curr. Microbiol.* **43**, 271–277 (2001).
24. R. Mukundan, "A new class of rotational invariants using discrete orthogonal moments," *Proc. 6th IASTED Conf. Signal Image Process.*, pp. 80–84 (2004).